1990

Mathematical Modeling of an H2S Removal Electrolyzer

Z. Mao
Texas A & M University - College Station

P. Adanuvor
Texas A & M University - College Station

Ralph E. White
University of South Carolina - Columbia

Publication Info

Journal of the Electrochemical Society, 1990, pages 2116-2123.

DOI: 10.1149/1.2086894
http://dx.doi.org/10.1149/1.2086894

r dimensionless deposition rate
$(S/V)_n$ surface to volume ratio, cm^{-1}
T dimensionless time, Eq. [9]
T_g gas temperature, K
T_1 power-on fraction of pulse period
T_2 power-off fraction of pulse period
T_p dimensionless pulse period, Eq. [9]
t time, s
u linear gas velocity, cm/s
UI uniformity index, Eq. [21]
x axial coordinate, cm

Greek

ϵ_{pss} error tolerance for detection of periodic steady state, Eq. [30]
θ time as a fraction of the pulse period during a single period
Λ radical diffusion length, cm
ξ dimensionless axial coordinate, Eq. [9]
ξ_j set of collocation points, Eq. [26]
τ gas residence time, Eq. [9]
τ_p pulse period, s

REFERENCES

1. D. M. Manos and D. L. Flamm, "Plasma Etching: An Introduction," Academic Press, New York (1989).
2. B. Chapman, "Glow Discharge Processes," John Wiley, New York (1980).
3. A. R. Reinberg, *J. Electron. Mater.*, **8**, 345 (1979).
4. A. Sherman, "Chemical Vapor Deposition for Microelectronics," Noyes Publications, Park Ridge (1987).
5. M. J. Kushner, *J. Appl. Phys.*, **63**, 2532 (1988).
6. R. J. Jensen, A. T. Bell, and D. S. Soong, *Plasma Chem. Plasma Process.*, **3**, 139 (1983).
7. C.-P. Chang, D. L. Flamm, D. E. Ibbotson, and J. A. Mucha, *J. Appl. Phys.*, **63**, 1744 (1988).
8. G. Turban and Y. Catherine, *Thin Solid Films*, **48**, 57 (1978).
9. G. Turban, Y. Catherine, and B. Grolleau, *ibid.*, **60**, 147 (1979).
10. I. Chen, *ibid.*, **101**, 41 (1983).
11. L. E. Kline, W. D. Partlow, and W. E. Bies, *J. Appl. Phys.*, **65**, 70 (1989).
12. R. S. Rosler and G. M. Engle, *Solid State Technol.*, p. 172, April 1981.
13. H. Y. Kumagai, in "Chemical Vapor Deposition 1984," McD. Robinson, G. W. Cullen, C. H. J. van den Brekel, J. M. Blocher, Jr., and P. Rai-Choudhury, Editors, p. 189, The Electrochemical Society Softbound Proceedings Series, PV 84-6, Pennington, NJ (1984).
14. L. J. Overzet, J. T. Verdeyen, R. M. Roth, and F. F. Carasco, *Mater. Res. Soc. Symp. Proc.*, **98**, 321 (1987).
15. Y. Watanabe, M. Shiratani, Y. Kubo, I. Ogawa, and S. Ogi, *Appl. Phys. Lett.*, **53**, 1263 (1988).
16. R. W. Boswell and R. K. Porteous, *J. Appl. Phys.*, **62**, 3123 (1987).
17. S. G. Hansen, G. Luckman, and S. D. Colson, *Appl. Phys. Lett.*, **53**, 1588 (1988).
18. S.-K. Park and D. J. Economou, *This Journal*, Submitted.
19. G. I. Taylor, *Proc. R. Soc. London, Ser. A*, **219**, 186 (1953).
20. W. R. Schmeal and N. R. Amundson, *AIChE J.*, **12**, 1202 (1966).
21. L. Lapidus and W. E. Schiesser, "Numerical Methods for Differential Systems," Academic Press, New York (1976).
22. B. A. Finlayson, "Nonlinear Analysis in Chemical Engineering," McGraw-Hill, New York (1980).
23. A. C. Hindmarch, in "Advances in Computer Methods for Partial Differential Equations • IV," R. Vichnevetsky and R. S. Stepleman, Editors, p. 312, IMACS, North Holland Publishing Co. (1981).
24. A. C. Hindmarch, in "Scientific Computing," R. Stepleman *et al.*, Editors, p. 55, IMACS, North-Holland Publishing Co. (1983).
25. A. C. Hindmarch, ACM-SIGNUM Newsletter, **15** (4), 10 (1980).
26. C. DeBoor, *SIAM J. Numer. Anal.*, **14**, 441 (1977).
27. D. Ramkrishna and N. R. Amundson, "Linear Operator Methods in Chemical Engineering with Applications to Transport and Chemical Reaction Systems," Prentice-Hall Inc., Englewood Cliffs, NJ (1985).
28. S.-K. Park and D. J. Economou, *J. Appl. Phys.*, **66**, 3256 (1989).
29. C. Ozgen and Z. Hicsasmaz, *Chem. Eng. Sci.*, **42**, 1413 (1987).
30. A. H. Wan and H. Y. Cheh, *This Journal*, **135**, 643 (1988).
31. H. B. Keller, in "Mathematical Aspects of Chemical and Biochemical Problems and Quantum Chemistry," D. S. Cohen, Editor, p. 85, American Mathematical Society, Providence, RI (1974).
32. K. F. Jensen and D. B. Graves, *This Journal*, **130**, 1951 (1983).

Mathematical Modeling of an H_2S Removal Electrolyzer

Z. Mao,* P. Adanuvor, and R. E. White****

Department of Chemical Engineering, Texas A&M University, College Station, Texas 77843

ABSTRACT

A mathematical model is presented for a high temperature H_2S electrolyzer. It is shown that the maximum current in this type of a cell is determined entirely by the transport rate of sulfide ions through the separator. It is suggested that this model could be used to determine the feasibility of various designs for this electrolyzer.

It has long been recognized that electrolysis of hydrogen sulfide (H_2S) would provide an effective means of cleaning various H_2S containing gases (1-3); consequently, a great deal of effort has been devoted to develop such a process. Unfortunately, electrolysis of H_2S in aqueous solutions leads to problems such as the passivation of the anode because of the deposition of sulfur (4), and the oxidation of sulfide or sulfur into sulfur oxyanions (5). The application of high temperature molten salts for this electrolysis may provide a means to overcome these problems because sulfur would be in a liquid or even a gaseous state at high temperatures, which would remove the "blocking" effect caused by elemental sulfur in the aqueous process. Also, because no oxygen would be present in the salts, neither sulfide nor other sulfur species would be oxidized into sulfur oxyanions. Several attempts have been made recently to use an electrolyzer similar to the molten carbonate fuel cell for this purpose (3, 6-8). While these experiments were carried out without much success, high polarization losses were experienced, the results of these experiments emphasized that improvement in the performance of these cells may be obtained by optimizing the cell design in a manner analogous to that for the molten carbonate fuel cell. Little attention has been paid to differences between these two types of electrochemical reactors. This work uses a mathematical model to examine the characteristics of the electrolyzer with regard to mass transport and to predict the maximum current density that could be obtained with this type of an electrolyzer.

Although the structure of the electrolyzer is similar to that of the molten carbonate fuel cell, the mass transport process is different from that of the molten carbonate fuel cell (MCFC). In the latter, the reactants are fed to both elec-

* Electrochemical Society Student Member.
** Electrochemical Society Active Member.

trodes from outside of the cell, where at the cathode O_2 reacts with the melt to generate CO_3^{2-} ions which carry the current to the anode. At the anode, the CO_3^{2-} ions react with H_2 gas to give water vapor and CO_2. In the MCFC, the polarization resistance at the cathode may control the overall reaction rate. For the proposed electrolyzer, the H_2S containing gas is fed to the cathode, where it reacts to produce hydrogen and sulfide ions

$$H_2S + 2e^- \rightarrow H_2 \uparrow + S^{2-} \quad [1]$$

The sulfide ions produced at the cathode must pass through the separator by migration and diffusion, and react at the anode to form sulfur

$$S^{2-} - 2e^- \rightarrow S \quad [2]$$

A simple calculation can illustrate how the maximum current density can be limited by the mass transport through the separator. Assuming that the effective diffusion coefficient of S^{2-} in the separator is 1.0×10^{-6} cm^2/s, the concentration of sulfide ions in the cathode is 1.0*M*, and a linear concentration profile exists in the separator for a separator of thickness 0.05 cm, the limiting current density can be estimated from Eq. [3] to be 3.8 mA/cm^2

$$i_{lmit} = 2\mathbf{F}D_{S^{2-}}\frac{C_{S^{2-}}}{h_s} \quad [3]$$

This limiting current density may be higher if migration is taken into account. Also, the concentration of sulfide ions in the cathode region may be much higher than 1.0*M*, and the concentration distribution may not be linear in the separator. Therefore, a more detailed analysis of the mass transport in the electrolyzer during the electrolysis is needed in order to determine the maximum current density as a function of the cell design and operating features of this electrolyzer.

Development of the Model

Figure 1 is a schematic representation of the proposed electrolyzer. The cathode is a sintered porous Ni-Cr plate. In the middle of the electrolyzer is a tape-cast lithium aluminate matrix which separates the electrodes and holds the electrolyte. The anode is assumed to be porous graphite. With this arrangement, H_2S is passed over the cathodic side where it dissolves in the melt and reacts according to Eq. [1]. The sulfide ions formed are then transported through the separator to the anode by diffusion and migration. At the anode, sulfide ions are oxidized into elemental sulfur which vaporizes at the back side of the electrode. The sulfur formed at the anode can react further with sulfide ions to form polysulfide species which can back-diffuse to the cathode. Consequently, hydrogen evolution would be partially replaced by reduction of the polysulfide ions to sulfide species. However, to simplify the model, these complications will not be considered, instead, a simple one-dimensional model will be developed to account for the transport processes taking place in the electrolyzer.

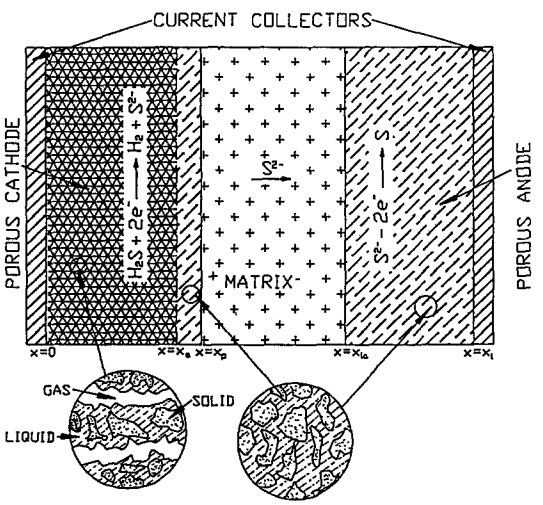

Fig. 1. Schematic of the electrolysis cell

An exploded view of the various regions of the electrolyzer is shown in Fig. 1. A three-phase reaction zone exists at the cathode towards the gas-side, whereas a two-phase reaction zone exists towards the matrix side of the cathode and in the anode. There are two phases in the separator as well, but it is assumed that no reaction occurs inside the separator.

Gas phase in the cathodic region.—The gas phase consists of two components, hydrogen and hydrogen sulfide. Hydrogen sulfide diffuses into the porous cathode, dissolves into the melt and reacts to form hydrogen gas according to reaction [1]. The mass balance for the two components can be expressed as follows (9)

$$\epsilon^g\frac{\partial C_i^g}{\partial t} = -\nabla \cdot N_i^g + R_{gi} \quad [4]$$

$$N_i^g = -C_t D_i^g \nabla X_i + X_i \sum_j N_j^g \quad [5]$$

where R_{gi} represents either the rate of the dissolution of hydrogen sulfide into the melt per unit volume of the electrode or the rate of the production of hydrogen gas per unit volume of the electrode. The other symbols in the equations are explained in the List of Symbols. The consumption rate of hydrogen sulfide per unit volume is equal to its diffusion rate into the bulk melt (10). It can expressed as

$$R_{g,H_2S} = -a^l D^c_{H_2S}\frac{\partial C_{H_2S}}{\partial \xi} \quad [6]$$

where a^l is the melt surface area per unit volume in the cathodic region. $D^c_{H_2S}$ is the diffusion coefficient of hydrogen sulfide in the melt, $\partial C_{H_2S}/\partial\xi$ stands for the derivative of the concentration of hydrogen sulfide at the melt surface in the direction normal to the surface which is approximately calculated by Eq. [7] on the basis of the thin film agglomerate model (11)

$$\frac{\partial C_{H_2S}}{\partial \xi} = \frac{C^*_{H_2S} - C_{H_2S}}{\delta} \quad [7]$$

where $C^*_{H_2S}$ and C_{H_2S} are the concentrations of the dissolved hydrogen sulfide at the melt surface and near the solid surface, respectively, and δ is the thin film thickness. It is assumed here that $C^*_{H_2S}$ is proportional to its concentration in the gas phase. That is

$$C^*_{H_2S} = K_H C^g_{H_2S} \quad [8]$$

Hydrogen gas that is produced in the cathode must penetrate through the gaseous pores in the cathode to the outside; the rate of hydrogen gas production is equal to its local electrode reaction rate, that is

$$R_{g,H_2} = -\frac{a_s^c i_c}{n\mathbf{F}} \quad [9]$$

where a_s^c is the specific surface area of the cathode, and i_c is the current density due to hydrogen evolution. In order to simplify Eq. [4] and [5], it is assumed that Knudsen diffusion is negligible and that there is no bulk gas flow in the x-direction. Therefore, the total pressure in the gas phase is constant, which when expressed in terms of concentration leads to the equation

$$C^g_{H_2S} + C^g_{H_2} = C_t \quad [10]$$

Equation [10] is used to simplify further Eq. [4] and [5], and the results are displayed in Table I.

Liquid phase in the cathodic region.—In the liquid phase of the porous cathode, the dissolved hydrogen sulfide is electrochemically reduced to form hydrogen gas and sulfide ions which are transported by migration and diffusion

Table I. Governing equations and boundary conditions

Gas phase in the porous cathode ($0 < x < x_a$)

$$\epsilon^g \frac{\partial C^g_{H_2}}{\partial t} = D^g_{H_2} \frac{\partial^2 C^g_{H_2}}{\partial x^2} - a_s{}^c \frac{i_c}{2F} \quad [I\text{-}1]$$

$$C^g_{H_2} + C^g_{H_2S} = C_t \quad [I\text{-}2]$$

Melt phase in the gas-fed porous cathode ($0 < x < l_a$)

$$\epsilon^c \frac{\partial C_{H_2S}}{\partial t} = D^c_{H_2S} \frac{\partial^2 C_{H_2S}}{\partial x^2} + a_s{}^c \frac{i_c}{2F} + a^l D^c_{H_2S} \frac{(K_H C^g_{H_2S} - C_{H_2S})}{\delta} \quad [I\text{-}3]$$

$$\epsilon^c \frac{\partial C_{S^{2-}}}{\partial t} = D^c_{S^{2-}} \frac{\partial^2 C_{S^{2-}}}{\partial x^2} - 2Fu^c_{S^{2-}} \left[\frac{\partial C_{S^{2-}}}{\partial x} \frac{\partial \phi}{\partial x} + C_{S^{2-}} \frac{\partial^2 \phi}{\partial x^2} \right] - a_s{}^c \frac{i_c}{2F} \quad [I\text{-}4]$$

where

$$i_c = i^\circ_{c,ref} \left(\frac{C_{S^{2-}}}{C_{S^{2-},ref}} \exp \left[\frac{-\alpha_c F}{RT} (E_c - \phi - U_{c,ref}) \right] - \frac{C_{H_2S}}{C_{H_2S,ref}} \exp \left[- \frac{(2 - \alpha_c)F}{RT} (E_c - \phi - U_{c,ref}) \right] \right) \quad [I\text{-}5]$$

$$\epsilon^c \frac{\partial C_i}{\partial t} = D_i{}^c \frac{\partial^2 C_i}{\partial x^2} + z_i F u_i{}^c \left[\frac{\partial C_i}{\partial x} \frac{\partial \phi}{\partial x} + C_i \frac{\partial^2 \phi}{\partial x^2} \right] \quad [I\text{-}6]$$

$$i = M^+, M^-$$

$$\sum z_i C_i = 0 \quad [I\text{-}7]$$

Melt phase in the porous cathode ($l_a < x < l_p$)

$$\epsilon^c \frac{\partial C_{H_2S}}{\partial t} = D^c_{H_2S} \frac{\partial^2 C_{H_2S}}{\partial x^2} + a_s{}^c \frac{i_c}{2F} \quad [I\text{-}8]$$

The equations for the other species are the same as Eq. [I-4]-[I-7]

In separating matrix region ($x_p < x < x_{la}$)

$$\epsilon^s \frac{\partial C_i}{\partial t} = D_i{}^s \frac{\partial^2 C_i}{\partial x^2} + z_i F u_i{}^s \left[\frac{\partial C_i}{\partial x} \frac{\partial \phi}{\partial x} + C_i \frac{\partial^2 \phi}{\partial x^2} \right] \quad [I\text{-}9]$$

for all species (see Table II)

$$\sum z_i C_i = 0 \quad [I\text{-}7]$$

In the porous anode region ($x_{la} < x < x_l$)

$$\epsilon^a \frac{\partial C_{S^{2-}}}{\partial t} = D^a_{S^{2-}} \frac{\partial^2 C_{S^{2-}}}{\partial x^2} - 2Fu^a_{S^{2-}} \left[\frac{\partial C_{S^{2-}}}{\partial x} \frac{\partial \phi}{\partial x} + C_{S^{2-}} \frac{\partial^2 \phi}{\partial x^2} \right] - a_s{}^a \frac{i_a}{2F} \quad [I\text{-}10]$$

where

$$i_a = i^\circ_{a,ref} \left(\frac{C_{S^{2-}}}{C_{S^{2-},ref}} \exp \left[\frac{\alpha_a F}{RT} (E_a - \phi - U_{a,ref}) \right] - \exp \left[- \frac{(2 - \alpha_a)F}{RT} (E_a - \phi - U_{a,ref}) \right] \right) \quad [I\text{-}11]$$

$$\epsilon^a \frac{\partial C_i}{\partial t} = D_i{}^a \frac{\partial^2 C_i}{\partial x^2} + z_i F u_i{}^a \left[\frac{\partial C_i}{\partial x} \frac{\partial \phi}{\partial x} + C_i \frac{\partial^2 \phi}{\partial x^2} \right] \quad [I\text{-}12]$$

for the other species (see Table II)

$$\sum z_i C_i = 0 \quad [I\text{-}7]$$

At $x = 0$

$$C^g_{H_2S} = C_t \quad [I\text{-}13]$$

$$C^g_{H_2} = 0 \quad [I\text{-}14]$$

$$C_{HS^-} = K_H C^g_{H_2S} \quad [I\text{-}15]$$

$$-D_i{}^c \frac{\partial C_i}{\partial x} - z_i F u_i{}^c C_i \frac{\partial \phi}{\partial x} = 0 \quad [I\text{-}16]$$

$$\sum z_i C_i = 0 \quad [I\text{-}7]$$

At $x = x_a$

$$\epsilon^g \frac{\partial C^g_{H_2}}{\partial t} = D^g_{H_2} \frac{\partial^2 C^g_{H_2}}{\partial x^2} - a_s{}^c \frac{i_c}{2F} \quad [I\text{-}17]$$

Continued

Table I. continued

At $x = x_p$

$$(1-\epsilon^c)\frac{i_c}{2\mathbf{F}} + \left(-D^c_{H_2S}\frac{\partial C_{H_2S}}{\partial x}\right)\Big|_{x=x_p^-} = \left(-D^s_{H_2S}\frac{\partial C_{H_2S}}{\partial x}\right)\Big|_{x=x_p^+} \quad [I\text{-}18]$$

$$-(1-\epsilon^c)\frac{i_c}{2\mathbf{F}} + \left(-D^c_{S^{2-}}\frac{\partial C_{S^{2-}}}{\partial x} + 2\mathbf{F}u^c_{S^{2-}}C_{S^{2-}}\frac{\partial \phi}{\partial x}\right)\Big|_{x=x_p^-} = \left(-D^s_{S^{2-}}\frac{\partial C_{S^{2-}}}{\partial x} + 2\mathbf{F}u^s_{S^{2-}}C_{S^{2-}}\frac{\partial \phi}{\partial x}\right)\Big|_{x=x_p^+} \quad [I\text{-}19]$$

$$i_c = i^\circ_{c,ref}\left(\frac{C_{S^{2-}}}{C_{S^{2-},ref}}\exp\left[\frac{\alpha_c\mathbf{F}}{RT}(E_c - \phi - U_{c,ref})\right] - \frac{C_{H_2S}}{C_{H_2S,ref}}\exp\left[-\frac{(2-\alpha_c)\mathbf{F}}{RT}(E_c - \phi - U_{c,ref})\right]\right) \quad [I\text{-}5]$$

$$\left(-D_i^c\frac{\partial C_i}{\partial x} + z_i\mathbf{F}u_i^cC_i\frac{\partial \phi}{\partial x}\right)\Big|_{x=x_p^-} = \left(-D_i^s\frac{\partial C_i}{\partial x} + z_i\mathbf{F}u_i^sC_i\frac{\partial \phi}{\partial x}\right)\Big|_{x=x_p^+} \quad [I\text{-}20]$$

$$i = M^+, M^-$$

$$\sum z_iC_i = 0 \quad [I\text{-}7]$$

At $x = x_{la}$

$$(1-\epsilon^a)\frac{i_a}{2\mathbf{F}} + \left(-D^a_{S^{2-}}\frac{\partial C_{S^{2-}}}{\partial x} + 2\mathbf{F}u^a_{S^{2-}}C_{S^{2-}}\frac{\partial \phi}{\partial x}\right)\Big|_{x=x_{la}^+} = \left(-D^s_{S^{2-}}\frac{\partial C_{S^{2-}}}{\partial x} + 2\mathbf{F}u^s_{S^{2-}}C_{S^{2-}}\frac{\partial \phi}{\partial x}\right)\Big|_{x=x_{la}^-} \quad [I\text{-}21]$$

$$i_a = i^\circ_{a,ref}\left(\frac{C_{S^{2-}}}{C_{S^{2-},ref}}\exp\left[\frac{\alpha_a\mathbf{F}}{RT}(E_a - \phi - U_{a,ref})\right] - \exp\left[-\frac{(2-\alpha_a)\mathbf{F}}{RT}(E_a - \phi - U_{a,ref})\right]\right) \quad [I\text{-}11]$$

$$\left(-D_i^a\frac{\partial C_i}{\partial x} + z_i\mathbf{F}u_i^aC_i\frac{\partial \phi}{\partial x}\right)\Big|_{x=x_{la}^+} = \left(-D_i^s\frac{\partial C_i}{\partial x} + z_i\mathbf{F}u_i^sC_i\frac{\partial \phi}{\partial x}\right)\Big|_{x=x_{la}^-} \quad [I\text{-}22]$$

$$\sum z_iC_i = 0 \quad [I\text{-}7]$$

At $x = x_l$

$$D_i^a\frac{\partial C_i}{\partial x} + z_iC_i\mathbf{F}u_i^a\frac{\partial \phi}{\partial x} = 0 \quad [I\text{-}23]$$

for all the species

$$\sum z_iC_i = 0 \quad [I\text{-}7]$$

into the separator. The effect of convection on mass transport is assumed to be negligible here because the electrode is quite thin, and the electrolyte is held in the matrix. The resulting mass balance for each species can be expressed by Eq. [11] (12)

$$\epsilon^c\frac{\partial C_i}{\partial t} = D_i^c\frac{\partial^2 C_i}{\partial x^2} + z_i\mathbf{F}u_i^c\frac{\partial}{\partial x}\left(C_i\frac{\partial \phi}{\partial x}\right) + R_{d,i} + R^c_{he,i} \quad [11]$$

$$i = 1, 2, \cdots, n$$

In the above equation, the concentration should be visualized as a volume averaged concentration, as discussed by Newman and Tiedemann (13). For the dissolved hydrogen sulfide, C_{H_2S} is different from $C^*_{H_2S}$. The first two terms on the right side of Eq. [11] result from the diffusion and migration. The third term is the result of hydrogen sulfide dissolution. For the dissolved hydrogen sulfide, it is expressed by Eq. [6], for those species which are not related with the dissolution of hydrogen sulfide into the solution, this term is zero. The fourth term is the net rate of the electrode reactions, and can be expressed by the equation

$$R^c_{he,i} = -a_s^c\sum_{j_c}\frac{s_{i_c}i_{j_c}}{n_{j_c}\mathbf{F}} \quad [12]$$

which is summed over the reaction occurring in the cathode only. The negative sign used in Eq. [12] is consistent with the conventions (12, 13), in which the stoichiometric coefficient of a reactant which is oxidized in an electrode reaction is positive, but negative otherwise. The current for an oxidation reaction is assigned a positive value, whereas that for a reduction reaction is assigned a negative value. Equation [11] represents a set of n equations with $n + 1$ unknowns (C_i, $i = 1, 2, \cdots, n$, ϕ). The relative concentrations of all ionic species at any point in the solution must satisfy the electroneutrality condition. That is

$$\sum z_iC_i = 0 \quad [13]$$

Equations [4], [10], [11]-[13] provide a complete set of the equations which are required to describe the mass transport process in the cathode region. The expanded forms of these equations are shown in Table I.

Separator region.—A solid phase and liquid phase are present in this region. The solid phase serves as an insulator separating the anode from the cathode. No electrode reaction takes place at the solid phase. The mass transport in this region is due to concentration gradients and a potential gradient across the separator. The governing equation for the mass balance of each species in this region can be expressed as

$$\epsilon^s\frac{\partial C_i}{\partial t} = -\nabla\cdot N_i \quad [14]$$

$$i = 1, 2, \cdots, n$$

Further expansion of this equation leads to Eq. [I-9] in Table I. Again, the electroneutrality condition is satisfied at points in this region.

Anode region.—Similarly to the separator region, there are two phases, solid phase and liquid phase. Electrode re-

actions take place at the solid phase. The general governing equations for the mass balance in this region are given by

$$\epsilon^a \frac{\partial C_i}{\partial t} = -\nabla \cdot N_i + R^c_{he,i} \quad [15]$$

where

$$R^a_{he,i} = -a_s{}^a \sum_{j_a} \frac{s_{ij_a} i_{j_a}}{n_{j_a} \mathbf{F}} \quad [16]$$

which is summed over the reactions occurring in the anode. An expanded form of this equation is presented in Table I.

Boundary conditions.—To solve the governing equations for the three regions, appropriate boundary and initial conditions must be specified. Overall, there are five interfaces (see Fig. 1) and the boundary conditions are specified as follows: At $x = 0$, it is assumed that the partial pressure of hydrogen gas is zero. This assumption implies that hydrogen sulfide gas is transported into the porous cathode at a maximum rate. In the liquid phase, the concentration of hydrogen sulfide is assumed to be in equilibrium with its partial pressure. For the other species in the solution, the flux of each species is zero. At $x = x_a$, it is assumed that H_2S gas diffuses into the electrolyte in the same way as at other positions and that no hydrogen is produced by the electrode reaction beyond this point. Therefore, the boundary conditions for the gas phase at this point are given by Eq. [I-2] and [I-17] in Table I.

The principle governing the boundary conditions at $x = x_p$ and $x = x_{la}$ is the continuity of flux at these interfaces. This leads to the following equations: at $x = x_p$

$$-(1 - \epsilon^c) \sum_{j_c} \frac{s_{ij_c} i_{j_c}}{n_{j_c} \mathbf{F}} \bigg|_{x=x_p} + N_i \bigg|_{x=x_p^-} = N_i \bigg|_{x=x_p^+} \quad [17]$$

at $x = x_{la}$

$$(1 - \epsilon^a) \sum_{j_a} \frac{s_{ij_a} i_{j_a}}{n_{j_a} \mathbf{F}} \bigg|_{x=x_{la}} + N_i \bigg|_{x=x_{la}^+} = N_i \bigg|_{x=x_{la}^-} \quad [18]$$

where N_i represents the flux of species i, the superscripts on x_p, etc., denote that the flux is evaluated from different directions. The first term on the left side of Eq. [17] and [18] is due to the electrode reaction occurring at the interfaces. These reactions take place only on the solid phase; consequently, the current should be multiplied by a fraction as shown in Eq. [17] and [18]. The different sign before the summations in Eq. [17] and [18] comes from the convention that the flux is positive in the x increasing direction. The expanded forms of these equations are listed in Table I. At the back side of the porous anode ($x = x_l$), it is assumed that no reaction takes place, and the flux of each species is zero. The equations for this boundary condition are also listed in Table II.

As a time-dependent problem, the initial conditions must be specified. It is assumed that the concentration distribution of each species is uniform cross the cell before a current is passed through the electrodes. That is, the initial concentration of each species is the same everywhere, equal to a given value. For the hydrogen gas, its initial concentration is zero.

A Butler-Volmer expression (14) is assumed to describe the relationship between the current density and the potentials for reactions [1] and [2] as shown below

$$i_j = i^\circ_{j,ref} \left\{ \prod_k \left(\frac{C_k}{C_{k,ref}} \right)^{p_{kj}} \exp \left[\frac{\alpha_{aj} \mathbf{F}}{RT} (E - \phi - U_{j,ref}) \right] \right.$$
$$\left. \prod_k \left(\frac{C_k}{C_{k,ref}} \right)^{q_{kj}} \exp \left[-\frac{\alpha_{cj} \mathbf{F}}{RT} (E - \phi - U_{j,ref}) \right] \right\} \quad [19]$$

The expression for an individual reaction is listed in Table I. If the electrolyte is not very conductive, in general, a supporting electrolyte is added to the melt to improve its conductivity and, consequently, to reduce the ohmic drop cross the cell. The conductivity of the melt will affect the potential distribution cross the cell and, therefore, the migration of sulfide ions through the separator. In order to take this factor into account, two pseudo ionic species M^+ and M^- are assumed to be present in the melt. The relationship between the conductivity of this melt and the concentrations of ionic species in the melt is given by Eq. [20] (12)

$$\kappa = \mathbf{F}^2 \sum_i u_i z_i{}^2 C_i \quad [20]$$

In summary, the equations that have been developed to describe the mass transport process in this electrolyzer are listed in Table I. The unknowns are $C^g_{H_2}$, $C^g_{H_2S}$, C_{H_2S}, $C_{S^{2-}}$, C_{M^+}, C_{M^-}, and ϕ. When the concentration distribution of each species and potential distribution cross the cell are obtained by solving these equations, the current density for a given cell voltage can be calculated either by summing up the flux of each species at any point in the separator region (Eq. [21]) or by integrating the current along the electrode (Eq. [22])

$$I = \sum_i^n z_i \mathbf{F} N_i \bigg|_{x=x_p^+} \quad [21]$$

$$I = a_s{}^c \sum_{j_c} \int_{x=0}^{x=x_p^-} i_{j_c} dx + (1 - \epsilon^c) \sum_{j_c} i_{j_c} \bigg|_{x=x_p} \quad [22]$$

Numerical Solution

An implicit finite difference method was used to solve the set of the equations listed in Table I and II, particularly the subroutine (BAND)(J)) developed by Newman (12) and the tridiagonal solver by Carnahan *et al.* (15) were used. The equations for the components in the gas phase and those for the species in the liquid phases were solved separately each time using the previous solutions as new guesses, the solution converged after a few iterations to satisfy the desired criteria. The fixed parameter values used in the program are listed in Table II.

Results and Discussion

Figure 2 shows the effect of electrolyte conductivity on steady-state polarization curves. The parameters used in this calculation are typical for a molten carbonate fuel cell. The effect of the conductivity is insignificant when the concentration of the supporting electrolyte is relatively high. However, when the conductivity decreases further,

Table II. Fixed input data

A. Parameters for electrode reactions

Reaction j	$i^\circ_{j,ref}$ (A/cm^2)	α_a	$U_{i,ref}$ (V)
$H_2S + 2e^- \rightarrow H_2 \uparrow + S^{2-}$	1.2×10^{-3}	1.0	0.062
$S^{2-} - 2e^- \rightarrow S$	1.3×10^{-3}	1.0	0.120

B. Transport properties and reference concentrations*

Species i	D_i (cm^2/s)	$C_{i,ref}$ (mol/l)	z_i
H_2 (g)	0.13	0.1	
H_2S (l)	1.2×10^{-5}	0.1	0
S^{2-}	1.2×10^{-5}	0.01	−2
M^+	1.3×10^{-5}	0.12	+1
M^-	1.2×10^{-5}	0.1	−1

C. Electrode structure parameters

Cell region	Porosity (ϵ)	Tortuosity (τ)	Thickness (h)
c	0.80	1.5	0.04 cm
s	0.80	1.5	0.02 cm
a	0.65	1.5	0.05 cm

* The mobilities of each species are calculated by $u_i = D_i/RT$, the effective diffusion coefficient for region j is calculated by $D_i^j = D_i \epsilon^j / \tau^j$. The other parameters are $K_H = 0.5$ and $a_s{}^1 = 1.0 \times 10^2$ cm^2/cm^3, $\delta = 1.0 \times 10^{-5}$ cm, $l_a \cong 0.035$ cm.

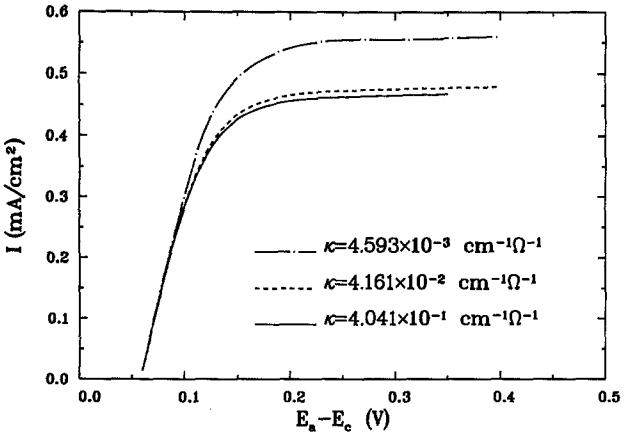

Fig. 2. The effect of conductivity on the polarization curve. $h_s = 0.06$ cm, $C^\circ_{H_2S} = 0.1M$, $C^\circ_{S^{2-}} = 1.0 \times 10^{-2}M$.

the limiting current increases appreciably. Evidently, a decrease in conductivity results in a greater potential gradient cross the separator; the driving force for migration of ionic species cross the separator increases, leading to an enhancement of the limiting current. The capability of using the electrolyzer for treating H_2S is related to the magnitude of the maximum current density through the cell. Unfortunately, for the design conditions considered here, the limiting current predicted from Fig. 2 is too low for any practical design of an electrolyzer for this process. The model could be used, however, to investigate other designs which may be practical.

The performance of the cell may be improved by changing the cell structure. One obvious approach to enhance the mass transport rate through the separator would be to make it much thinner. Figure 3 demonstrates how much the limiting current can be increased by reducing the separator thickness within a realistic range. Although the maximum current density increases significantly when the separator thickness is reduced, the current is still far lower than that one would want for industrial electrolysis. One of other properties of the separator could be modified to improve the cell is its porosity. As shown in Fig. 4, the limiting current density varies linearly with the porosity. Therefore, the performance of the cell could not be significantly improved by changing the separator porosity.

Figure 5 shows the concentration distribution of sulfide ions cross the cell at different times. Initially, concentration gradients appear only cross the interfaces between the separator and electrodes. However, after some time, there is a rapid rise in the concentration of sulfide ions at the cathode as a result of reaction [1], and a corresponding drop in concentration of S^{2-} ions at the anode as a consequence of reaction [2]. As time increases, the concentration profile of S^{2-} ions cross the separator changes accordingly. After a long time, a steady-state profile develops across the

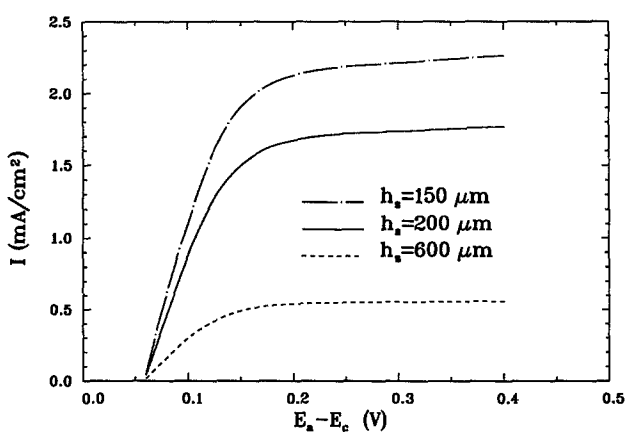

Fig. 3. The effect of the separator thickness on the polarization curve. $C_{S^{2-}} = 0.01M$, $C_{H_2S} = 0.1M$, $\kappa = 4.593 \times 10^{-3}$ cm^{-1} Ω^{-1}.

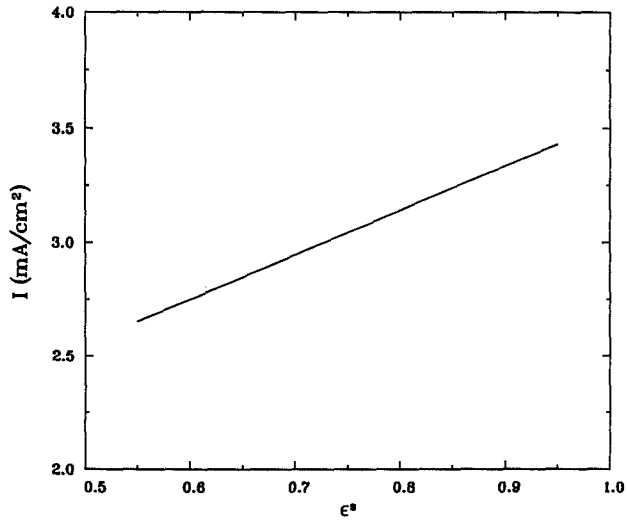

Fig. 4. The effect of the separator porosity on the current density. $E_a - E_c = 0.4$V, $C_{S^{2-}} = 0.01M$, $C_{H_2S} = 0.1M$, $\kappa = 4.593 \times 10^{-3}$ cm^{-1} Ω^{-1}, $h_s = 0.02$ cm.

cell, with the profile in the anodic region indicating a nearly complete consumption of S^{2-} ions in the vicinity of the anode. These concentration profiles as a function of time can be further explained in terms of the potential profile cross the cell. Figure 6 shows changes in the potential profile with time. The reaction rate is controlled initially by the ohmic resistance in the separator. Consequently, there is a drastic change in potential cross the separator. As Fig. 6 shows, the driving force for the electrode reactions occurring at both the anode and the cathode is higher near the interfaces than in the electrodes, resulting in higher reaction rates at these places. Consequently, the S^{2-} concentration gradient appears first near the interfaces, as shown in Fig. 5. As time elapses, the concentration polarization for the anodic reaction becomes more and more significant because of the limiting transport rate through the separator, leading to a corresponding potential shift in the solution in the negative direction. After a steady state has been established, the potential profile in the solution becomes nearly flat and entirely shifts to the cathodic side. When this happens, almost the whole cell voltage is used to overcome the concentration polarization of the anodic reaction, the reactant transferred from the cathode is con-

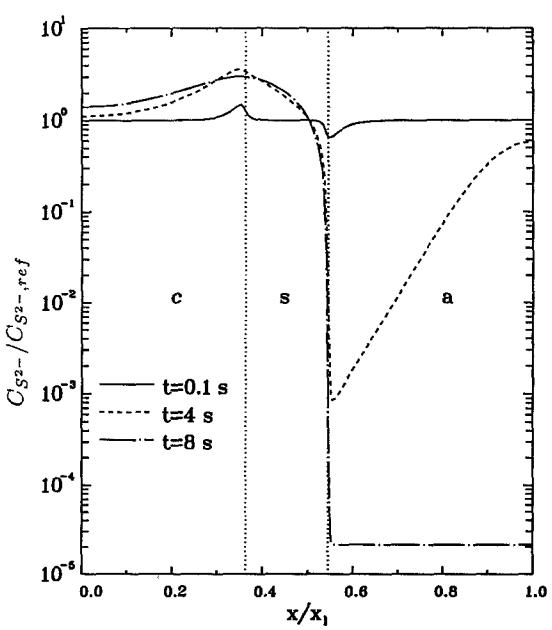

Fig. 5. The S^{2-} concentration profile cross the cell. $E_a - E_c = 0.4$V, $C_{S^{2-}} = 0.01M$, $C_{H_2S} = 0.1M$, $h_s = 0.02$ cm, $\kappa = 4.593 \times 10^{-3}$ cm^{-1} Ω^{-1}.

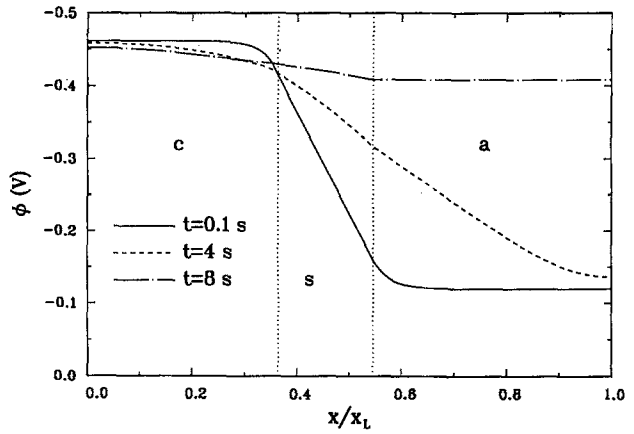

Fig. 6. The potential profile in the solution cross the cell. $E_a - E_c = 0.4V$, $C_{S^{2-}} = 0.01M$, $C_{H_2S} = 0.1M$, $h_s = 0.02$ cm, $\kappa = 4.593 \times 10^{-3}$ cm^{-1} Ω^{-1}.

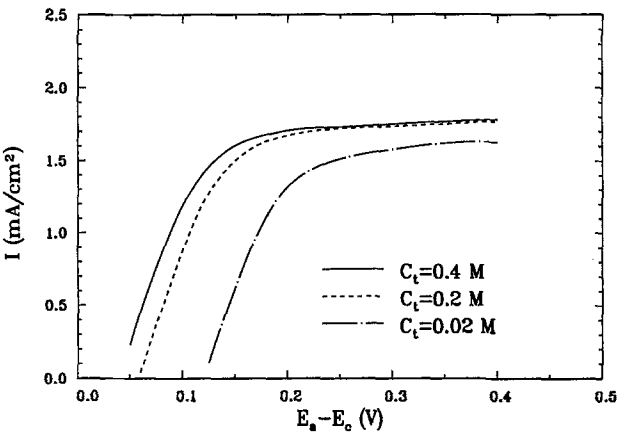

Fig. 8. The effect of the H_2S concentration on the polarization curve. $\kappa = 4.593 \times 10^{-3}$ cm^{-1} Ω^{-1}.

sumed predominantly near the interface between the separator and the anode, and the concentration of S^{2-} ions in the anodic region becomes almost zero. Figure 7 shows the current density distribution along the anode as a function of time. The current density changes linearly with the position at time $t = 0.1$s when the concentration polarization is negligible and the potential profile is linear as shown in Fig. 5 and 6. With time increasing, the concentration polarization develops, the current density distribution changes accordingly. Finally, the current becomes very small inside of the electrode, and predominates in the front side of the electrode.

An increase in H_2S pressure may result in a significant increase in the limiting current density as is normally the case in fuel cells. If this is true, one can select an electrolyte which has a high solubility for H_2S. Figure 8 shows the effect of H_2S pressure on the polarization curves. An increase in H_2S pressure causes a shift of the rest potential and only a slight increase in the maximum current density. It should be realized that transport rate of reactants into the electrodes normally controls the overall reaction rate in the case of fuel cells, whereas in this electrolyzer, the transport of sulfide ions through the separator limits the reaction rate. An increase of H_2S pressure only increases the activity of dissolved H_2S in the melt, not necessarily the concentration of sulfide ions. The concentration of S^{2-} ions in the cathodic region depends mainly on the charge passed through the cell. As stated previously, the current is controlled predominantly by the ohmic resistance in the separator region in a relatively short time after a potential is applied. The concentration of S^{2-} ions in the cathodic region could not be built up by one or two orders of magnitude or even many folds within this time period. Therefore, when the S^{2-} ions in the anodic region are completely consumed, the high resistance to mass transport in the separator region keeps the rate of transport of S^{2-} ions to the anode region small.

Since the overall reaction rate is entirely controlled by the transport rate of S^{2-} ions through the separator, it can be expected that changes in electrode structural parameters such as porosity and specific electrode areas will do little to enhance the performance of the electrolyzer. Figure 9 and 10 demonstrate the effects of the respective specific surface areas of the anode and cathode on the current density. The specific area affects only the transient currents, but shows practically no effect on the steady-state current densities.

Conclusions

A mathematical model has been presented to examine the concept of using an electrolyzer similar to the molten carbonate fuel cell for electrolysis of hydrogen sulfide. Under the conditions assumed in this model, the maximum current density with this type of cell is determined by the reactant transport rate through the separator. A significant portion of the cell voltage is used to overcome the concentration polarization in the anodic region. The concentration of sulfide ions in the cathodic region cannot be increased by many orders of magnitude after a current has been passed through the cell, on the other hand, the concentration of S^{2-} ion in the anodic region is limited by the

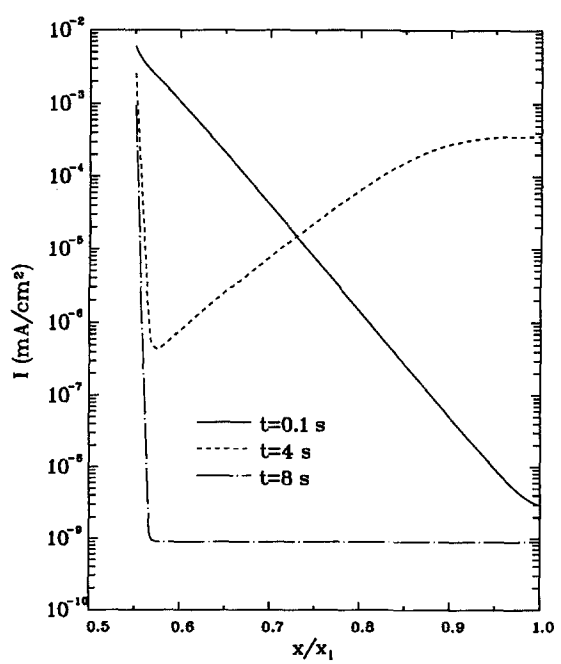

Fig. 7. The current transferred per unit volume as function of position along the anode. $E_a - E_c = 0.4V$, $C_{S^{2-}} = 0.01M$, $C_{H_2S} = 0.1M$, $h_s = 0.02$ cm, $\kappa = 4.593 \times 10^{-3}$ cm^{-1} Ω^{-1}.

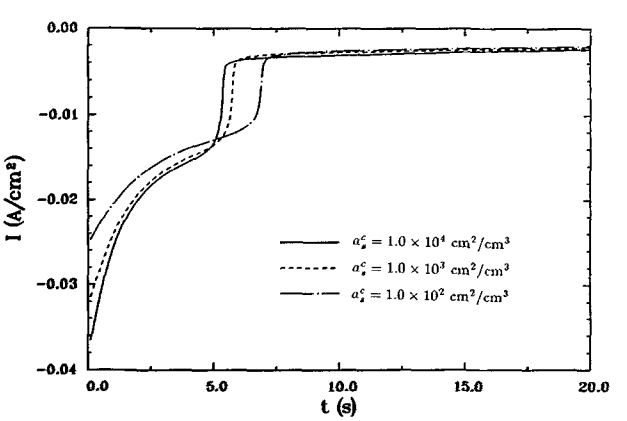

Fig. 9. The effect of cathode specific area on the current-time curve. $E_a - E_c = 0.4V$, $C_{S^{2-}} = 0.01M$, $C_{H_2S} = 0.1M$, $\kappa = 4.593 \times 10^{-3}$ cm^{-1} Ω^{-1}, $a_s^a = 1.0 \times 10^4$ cm^2/cm^3.

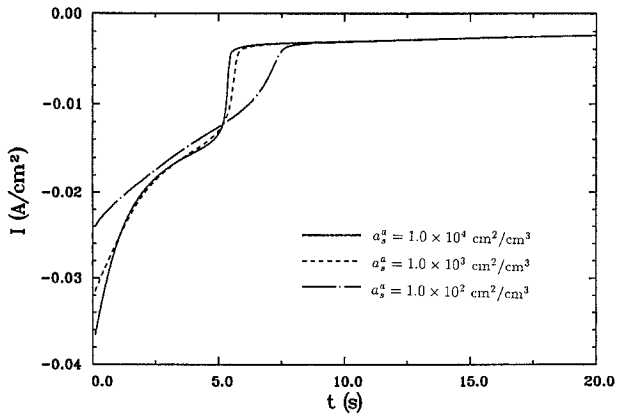

Fig. 10. The effect of the anode specific area on the current-time curve. $E_a - E_c = 0.4V$, $C_{S^{2-}} = 0.01M$, $C_{H_2S} = 0.1M$, $\kappa = 4.593 \times 10^{-3}$ cm^{-1} Ω^{-1}, $a_s^c = 1.0 \times 10^4$ cm^2/cm^3.

resistance to mass transport in the separator region. Therefore, under the most optimistic conditions, the maximum current density for this type of electrolyzer cannot be improved beyond 10 mA/cm^2, a value that is far too small for any practical large scale industrial applications. The model could be used to study fundamentals (obtain values for effective diffusion coefficients, *e.g.*) of the processes occurring in a laboratory scale electrolyzer. Such information may be useful to development of molten carbonate electrolyte and alkaline electrolyte fuel cells.

Manuscript submitted Aug. 31, 1989; revised manuscript received *ca.* Jan. 15, 1990.

Texas A&M University assisted in meeting the publication costs of this article.

LIST OF SYMBOLS

a_s^i specific surface area of the region, i, cm^2/cm^3
C_i^g concentration of component i in the gas phase, mol/cm^3
C_i concentration of species i in the liquid phase, mol/cm^3
$C_{i,ref}$ reference concentration of species i, mol/cm^3
C_i^o initial concentration of species i, mol/cm^3
C_t total concentration of the gas phase, mol/cm^3
D_i diffusion coefficient of species i, cm^2/s
D_i^k effective diffusion coefficient of species i in region k, cm^2/s
E_a anode potential, V
E_c cathode potential, V
$\mathbf{F}$ Faraday's constant, 96,487 C/mol
h_a the thickness of the anode, cm
h_c the thickness of the cathode, cm
h_s the thickness of the separator, cm
I current density, A/cm^2
i_j current density due to electrode reaction j, A/cm^2
$i^o_{j,ref}$ exchange current density at reference concentrations for reaction j, A/cm^2
i_{limit} limiting current density, A/cm^2
K_H constant (see Eq. [8])
n_j number of electrons transferred in reaction j
N_i flux of species i, mol/cm^2-s
N_i^g flux of species i in the gas phase, mol/cm^2-s
p_{ij} anodic reaction order of species i in reaction j
q_{ij} cathodic reaction order of species i in reaction j
R universal gas constant, 8.314 J/mol-K
$R^k_{he,i}$ heterogeneous reaction rate with respect to species i for the reaction k, mol/cm^3-s
$R_{d,i}$ change rate of the concentration of species i due to the dissolution of hydrogen sulfide, mol/cm^3-s
s_{ij} stoichiometric coefficient of species i in reaction j
T absolute temperature, K
t time, s
u_i^k effective mobility of species i in region k, mol-cm^2/J-s
$U_{j,ref}$ theoretical open-circuit potential evaluated at reference concentrations, V
X_i molar fraction of component i in the gas phase
x_a thickness of gas, liquid and solid co-existence region in the cathode, cm
x_p thickness of the cathode, cm
x_{la} thickness of the cathode plus the separator, cm
x_l total thickness of the electrolyzer, cm
z_i charge number of species i

Greek symbols

α_{aj} transfer coefficient for reaction j
δ the thickness of liquid film covering on the solid agglomerates in the cathode, cm
ϵ^k porosity of region k
κ conductivity of the melt, cm^{-1} Ω^{-1}
ξ coordinator in the direction normal to the liquid surface in the cathode, cm
τ^k tortuosity of region k
ϕ potential in solution, V

Superscript or subscripts

a anodic, anodic region
c cathodic, cathodic region
g gas phase
l liquid phase
s separator region

REFERENCES

1. J. E. Noring and E. A. Fletcher, *Energy*, **7**, 651 (1982).
2. K. Nygren, W. H. Smyrl, E. A. Fletcher, and R-T, Atanasaski, Abstract 549, p. 788, The Electrochemical Society Extended Abstracts, Atlanta, GA, May 15-20, 1988.
3. R. W. Bartlett, D. Cubicciotti, D. L. Hildenbrand, D. D. Macdonald, K. Semran, and M. E. D. Raymand, SRI Project Final Report, No. 8030, July 1979.
4. P. W. Bolmer, U.S. Pat., No. 3,409,520, Nov. 1968.
5. S. I. Zhdanow, in "Encyclopedia of Electrochemistry of the Elements," Vol. 6, A. J. Bard, Editor, Marcel Dekker, Inc., New York (1982).
6. H. S. Lim and J. Winnick, *This Journal*, **131,** 562 (1984).
7. D. Weaver and J. Winnick, *ibid.*, **134,** 2451 (1987).
8. J. Winnick, U.S. Pat., No. 4,772,366, Sept. 1988.
9. R. B. Bird, W. E. Steward, and E. N. Lightfoot, "Transport Phenomena," John Wiley & Sons, Inc., New York (1960).
10. P. V. Danckwerts, "Gas-Liquid Reactions," McGraw-Hill, Inc., New York (1970).
11. R. P. Iczkowski and M. B. Cutlip, *This Journal*, **127,** 1433 (1980).
12. J. Newman, "Electrochemical Systems," Prentice-Hall, Inc., Englewood Cliffs, NJ (1973).
13. J. Newman and W. Tiedemann, *AIChE J*, **21,** 25 (1975).
14. R. E. White, S. E. Lorimer, and R. Darby, *This Journal*, **130,** 1123 (1983).
15. R. Carnahan, H. A. Luther, and J. O. Wilkes, "Applied Numerical Methods," John Wiley & Sons, Inc., New York (1969).